International Journal of Heat and Mass Transfer 212 (2023) 124298

Contents lists available at ScienceDirect

International Journal of Heat and Mass Transfer

journal homepage: www.elsevier.com/locate/hmt

Multi-objective optimization on bionic fractal structure for heat exchanging of two fluids by genetic algorithm

Lisheng Pan[a,b,*], Zikang Yao[a,b], Wei Yao[a,b], Xiaolin Wei[a,b]

[a] State Key Laboratory of High-Temperature Gas Dynamics, Chinese Academy of Sciences, Institute of Mechanics, Beijing 100190, China
[b] School of Engineering Sciences, University of Chinese Academy of Sciences, Beijing 100049, China

ARTICLE INFO

Article history:
Received 28 December 2022
Revised 3 April 2023
Accepted 9 May 2023
Available online 22 May 2023

Keywords:
Bionic fractal structure
Thermo-hydraulic performance
Heat transfer enhancement
Genetic algorithm optimization

ABSTRACT

Numerous industrial processes involve heat exchange, and the efficiency of energy usage depends heavily on the effectiveness of this exchange. Thermal structure is a critical factor that influences the process of heat transfer. The bionic fractal structure has been heavily researched due to its ability to provide a more uniform flow distribution and improved heat transfer performance. An iterative approach to determining the central wall temperature is suggested for heat transfer between two fluids with varying mass flow rates and physical features. A bionic fractal heat transfer model for two fluids was developed, and the features of the bionic fractal heat transfer structure with supercritical carbon dioxide (supercritical CO_2) and H_2O were expounded. Furthermore, the variation of heat transfer performance with parameters was analyzed comprehensively. A method for the optimization and design of a bionic fractal heat transfer structure using two fluids was also provided, and the index of heat transfer performance was found to have the best value for various structural factors. The multi-objective optimizations of the bionic fractal heat transfer structure were carried out by a genetic algorithm, and the results showed a 15% reduction in power consumption for the optimized heat transfer structure, a 2.4% increase in heat transfer, and an improvement in the index of heat transfer performance by 17%.

1. Introduction

Heat transfer processes are prevalent in various industries and applications, including nuclear power, shipbuilding, electronic communication, electricity, aerospace, and other fields [1]. The heat transfer performance significantly affects the efficiency of energy utilization, making the technology of heat transfer enhancement critical in improving energy efficiency and increasing economic benefits.

There are two approaches to heat transfer enhancement: active and passive. Active heat transfer enhancement involves additional equipment, which limits its development due to its complexity and increased energy consumption. On the other hand, passive heat transfer enhancement focuses on the optimization and design of flow channel structures, which achieves higher heat transfer performance with high stability without requiring additional equipment. Scholars have carried out significant research on various flow channel structures such as zigzag, S-shaped, fin-shaped, and wing-shaped. Printed circuit heat exchanger (PCHE) is often combined with different flow channel structures to achieve higher heat transfer performance due to its much higher heat flux [1]. Ishizuka et al. [2] studied the heat transfer performance of zigzagged heat transfer structures and established an empirical fitting formula for pressure loss and heat transfer. Dong et al. [3] discovered that a sawtooth channel heat transfer structure has superior heat transfer performance but has a pressure drop caused by resistance at the corner. Kim et al. [4] showed that the Nusselt number of sawtooth heat exchange structures increases by 50% with an increase in the channel inclination angle. Ngo et al. [5] pointed out a positive correlation between heat transfer and pressure drop of microchannel heat transfer structures with S-shaped and sawtooth channels, but S-shaped channels achieve lower pressure drops. To enhance heat transfer performance, Ngo et al. [6] proposed an S-shaped fin channel, which significantly reduces volume and pressure drop. Tsuzuki et al. [7] introduced the heat transfer characteristics of S-channel and sawtooth heat transfer structures and found that, under similar heat transfer capacities, the pressure drop produced by an S-channel heat transfer structure is only 1/5 that of the sawtooth heat transfer structure. Kim et al. [8] analyzed the hydraulic and thermal performance of a sinusoidal PCHE and showed that the heat transfer effect is significantly improved by adding a wing spoiler. The fin arrangement in PCHE with an airfoil was optimized

* Corresponding author at: State Key Laboratory of High-temperature Gas Dynamics, Institute of Mechanics, Chinese Academy of Sciences, Beijing 100190, China.
E-mail address: panlisheng@imech.ac.cn (L. Pan).

https://doi.org/10.1016/j.ijheatmasstransfer.2023.124298
0017-9310/

Nomenclature

A	heat transfer area (m^2)
c	specific heat capacity ($kJ \cdot kg^{-1} \cdot °C^{-1}$)
d	hydraulic diameter (m)
E	index of heat transfer performance
F	resistance loss (m)
f	turbulent resistance coefficient
h	convective heat transfer coefficient ($W \cdot m^{-2} \cdot K^{-1}$)
i	infinitesimal section number
j	total number of segments
k	fractal series
l	length (m)
$\dot{m}$	mass flow rate ($kg \cdot s^{-1}$)
n	number of branches
Nu	Nusselt number
Pr	Prandtl number
Q	quantity of heat (W)
R	thermal resistance ($m^2 \cdot K \cdot W^{-1}$)
Re	Reynold number
t	temperature (°C)
u	velocity ($m \cdot s^{-1}$)
W	power consumption (W)

Subscript

c	cold fluid side
h	hot fluid side
w	wall side
LMTD	logarithmic mean

Superscripts

'	inlet
''	outlet

Greek letters

β	length ratio
γ	diameter ratio
δ	thickness of the wall (m)
ε	local resistance coefficient
ζ	drag coefficient along the path
λ	thermal conductivity coefficient ($W \cdot m^{-1} \cdot K^{-1}$)
μ	dynamic viscosity coefficient
ρ	density ($kg \cdot m^{-3}$)

by Xu et al. [9], reducing flow resistance by 22.8%. Chen et al. [10] compared the heat transfer capacities of an airfoil structure and a zigzag channel and found that the airfoil structure improved by 29.93%. However, the flow in the structure of the microchannel has great instability when working conditions change. Zhang et al. [11] found that the uneven distribution of the medium seriously affects the overall heat transfer structure through studying straight channels. Kim et al. [12] found that the uneven flow distribution of the medium in heat exchange equipment causes the operating time of equipment to decrease.

Biomimetic fractal networks are widely found in nature, such as in the respiratory and circulatory systems of animals and the transport systems of plants. These fractal structures have evolved over a long period and offer several advantages, such as uniformity of the transport medium, low flow resistance, and high efficiency of heat and mass transfer. As illustrated in Fig. 1, the distribution of tree roots and blood vessels show these biomimetic fractal structures, which exhibit superior energy transfer efficiency and low flow resistance, can be employed in flow and heat transfer systems. Pence et al. [13] introduced the heat transfer performance of bionic fractal structures and found that resistance is reduced by about 60% when compared to a parallel structure. At each bifurcation in the fractal structure, the flow and heat transfer boundary layers are interrupted and reformed, and the periodic disturbance of the fractal level strengthens the heat transfer process. However, further research is needed on heat transfer and power consumption. Under the same heat transfer area, Ma et al. [14] pointed out that the pressure drop of a Y-shaped bionic micro-flow channel is reduced by 37.67% compared with a parallel flow channel. Meanwhile, the average temperature of the heat source surface decreases by 7.66°C, and the maximum temperature difference also decreases by 6.51°C. However, the hydraulic characteristics of multi-branches were not further studied. Wang et al. [15] suggested that the tree-shaped fractal structure is less affected by flow blockage, and the influence of branches is further studied. However, global optimization is still needed. Drawing on biomimetic fluid mechanics, researchers have designed fractal micro-channel radiators, such as dish [16], tree [17], Y-type [18], H-shaped [19], and wing vein type [20], based on naturally optimized transport systems. It is shown that the fractal micro-channel radiator has better capabilities for heat radiation and even temperature, and effectively reduces the pressure drop. However, due to the complexity of the fractal structure, its optimization is not effectively addressed.

In recent years, there has been significant research on fractal structures. Tang et al. [22] demonstrated that the use of higher-order fractals at the end of the fractal microchannel can decrease surface temperature by 4 K. Ji et al. [23] studied and optimized different bifurcation angles and achieved a reduction in pressure drop of over 50%. Yan et al. [24] optimized the flow distribution of a double-layered heat sink, which resulted in further improvements in cooling performance. However, these studies have all focused on the design and optimization of single-fluid heat transfer structures. Double-fluid heat transfer systems are widely used in various industrial processes, making their optimization and design critical. Thus, urgent attention is required to carry out the optimization and design of double-fluid bionic fractal heat transfer structures. The supercritical CO_2 Brayton cycle, due to its high cycle efficiency [25], wide range of applications, and great potential, presents a significant opportunity for the use of micro-channel heat transfer structures. Its working medium also has better liquidity and small viscosity [26], leading to significant reductions in power consumption and the achievement of higher cycle efficiency. Therefore, the optimization and design of supercritical CO_2 heat transfer structures hold great significance.

To summarize, we propose a novel double fluid bionic fractal heat transfer structure that uses supercritical CO_2 and H_2O. We establish a model for this structure and develop a thermal design procedure that is suitable for various flow rates, pipe diameters, and physical properties of the medium. By addressing gaps in previous research, we conduct a comprehensive analysis of the heat transfer performance of the supercritical CO_2 and H_2O bionic fractal heat transfer structure by controlling flow rate, structure parameters, and inlet parameters. Finally, we perform multi-objective optimizations to obtain the optimal configuration of the bionic fractal heat transfer structure in terms of both thermal and hydraulic performance.

2. Methodology

The LMTD method and the NTU method are commonly used for thermal design of heat exchange structures. Jolly et al. [27] designed a calculation program for micro-element to obtain heat transfer and pressure drop of tubular heat exchangers. Lian et al. [28] adopted the segmental LMTD method for the precooler of a straight channel, and Saeed et al. [29] compared the results of segmental thermal design with numerical simulation to verify the re-

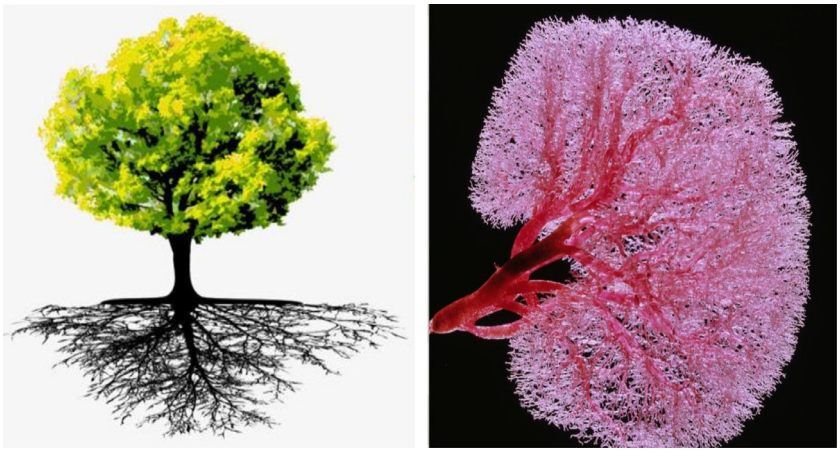

Fig. 1. Fractal flow channel in nature [21].

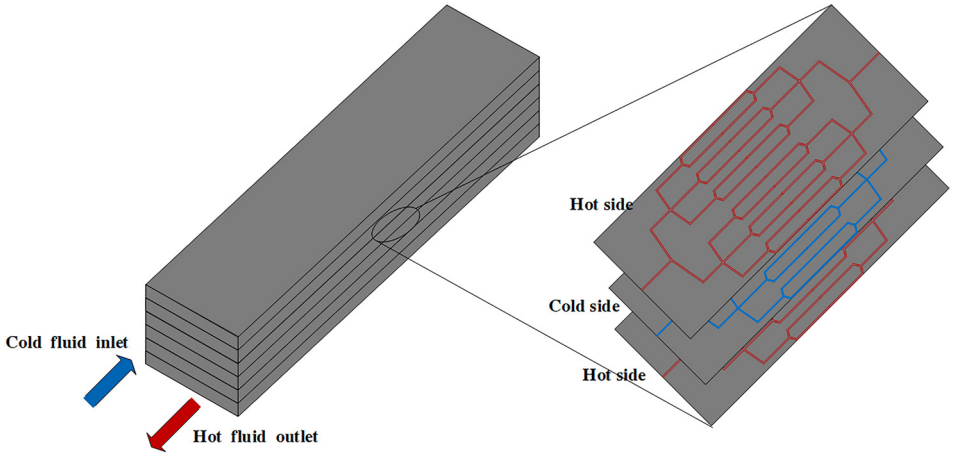

Fig. 2. Model of fractal heat transfer structure.

liability of thermal design methods. However, the NTU method and the LMTD method cannot be directly applied to the thermal design of bionic fractal heat transfer structures. On the one hand, physical properties of the medium, such as supercritical CO_2 and hydrocarbon fuel, vary sharply with temperature and pressure, while mass flow changes with fractal level in bionic fractal heat transfer structures. On the other hand, conventional design of heat exchanger structures is mostly limited by parameters of inlet and outlet, heat and pressure drop. In complex fractal structures, only the inlet parameters of working medium are taken as constraints, so the time cost of LMTD calculation is too high. To accurately describe heat and power consumption and reduce the time cost of calculation, a design method of wall temperature iteration suitable for complex heat transfer structures is adopted. This method divides the flow channel into 50 segments and, compared to the LMTD method, accelerates the calculation time by 10 times while the design space coverage does not have excessive limitations. Under different design scales, appropriate heat transfer relationships are selected based on different heat transfer scales.

2.1. Model of fractal heat transfer structure

The fractal heat transfer structure consists of cold and hot fluid channels, as shown in Figs. 2 and 3. To simplify the computational model, we assume that the bifurcation channel is uniform at each branch and that local resistance is only related to the number of branches. The channel layout on the left side is symmetrical to that on the right side.

Each microtubule is treated as a computational unit, and heat and power consumption of each section were calculated piecewise to obtain the heat and power consumption of the heat transfer structure. The basic assumptions used in the calculation of each segment are as follows.

(1) The mass flow rate and specific heat capacity of cold and hot fluids in microtubes remain constant over the entire heat transfer surface.
(2) The heat transfer coefficient of the microtube is uniform over the entire heat transfer surface.
(3) The heat transfer structure does not experience heat loss.
(4) Thermal conduction along the axial direction of the pipe in the heat transfer process can be neglected.

The structural parameters of a heat transfer structure have a significant impact on its heat transfer performance. Therefore, appropriate optimization methods are required to obtain the optimal structural parameters. One such method is the Genetic Algorithm (GA), which is a global stochastic optimization algorithm based on natural selection and genetic mechanisms [30].

During the optimization calculation process, a random population is initially generated and potential solutions are coded as chromosomes. The fitness of each individual is then calculated, which represents the objective evaluation of the solution. Individuals with higher fitness have a higher probability of being saved for the next generation. To maintain diversity within the population, new chromosomes are generated by crossover between each chromosome. Additionally, chromosomes in the population are mutated

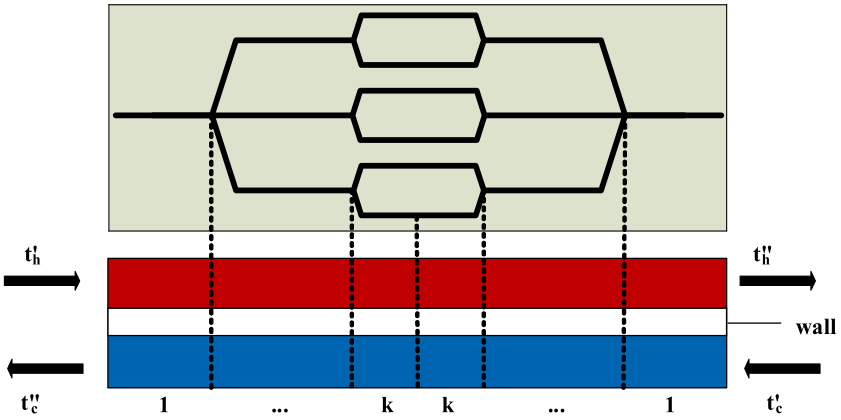

Fig. 3. Pipe heat transfer and flow diagram.

with a certain probability. These genetic operations, including selection, crossover, and mutation, are repeated until the population evolves in the direction of producing a better next generation. This process continues until the optimal solution that meets the design requirements is obtained.

To address the optimization and design challenges of biomimetic fractal structure, a program for heat exchange structure optimization and design is established, as illustrated in Fig. 4. The program consists of three main parts. The first part is the main program of the genetic algorithm, which employs the elite strategy to increase the probability of selecting the fittest solutions for the next generation. The second part is Program A, which integrates the calculation results of the bionic fractal model into the heat transfer performance target for genetic operations. Finally, the third part comprises Programs B and C for heat transfer structure, which utilize the central wall temperature method.

Detailed steps for the third part are given below.

Step 1: Input the structural parameters of the fractal structure, including the pressure and temperature of the inlet, the mass flow rates of the cold and hot fluids at the inlet, and select the length of the micro-pipe segments and the total number of segments *j*.

Step 2: Make an initial guess for the central wall temperature of each microtubule, $T_{w,\,i}$.

Step 3: Make an initial guess for the average pressure and temperature at the first section of the hot fluid. Calculate the heat transfer, pressure drop, temperature drop, and temperature and pressure at the outlet of the first section using Eqs. (1) and (2). In the calculation of this stage, the fluid temperature drop and pressure drop of the micro-element segment are iteratively revised until the given residual error is met.

Step 4: From left to right, take the outlet parameters of section *i* as the inlet parameters of section *i*+1 in turn. Calculate the heat transfer parameters of each segment iteratively. Repeat this process for the side of the cold fluid.

Step 5: Compare whether the heat transfer of the cold and hot fluids in each micro-element segment meets the requirements. If not, adjust the wall temperature of each segment to obtain a new set of wall temperatures, and repeat step 2 until the requirements are met.

2.2. Basic equations of thermal design

The heat balance equation of each section is as follows.

$$Q = \dot{m}_h \cdot c_h \cdot \left(t'_h - t''_h\right) = \dot{m}_c \cdot c_c \cdot \left(t''_c - t'_c\right) \tag{1}$$

The heat transfer equation of logarithmic temperature difference is given by following relations.

$$Q = \frac{\Delta T_m}{R} \tag{2}$$

The logarithmic mean temperature difference is as follows.

$$\Delta T_1 = \left|t' - t_w\right| \tag{3}$$

$$\Delta T_2 = \left|t'' - t_w\right| \tag{4}$$

$$\Delta T_m = \frac{\Delta T_1 - \Delta T_2}{ln\left(\frac{\Delta T_1}{\Delta T_2}\right)} \tag{5}$$

The thermal resistance of hot and cold side can be calculated by following relations.

$$\frac{1}{R} = \frac{1}{h \cdot A} + \frac{\delta}{2 \cdot \lambda_w \cdot A_w} \tag{6}$$

The convective heat transfer coefficient on hot and cold side of each segment is defined by following relations.

$$h = \frac{Nu \cdot \lambda_f}{l} \tag{7}$$

The Nusselt number of each segment is determined by empirical heat transfer correlation. Considering entrance effect section, when flow is laminar, Nusselt number adopts the Sieder-Tate correlation.

$$Nu = 1.86 \cdot (Re \cdot \mathrm{Pr} \cdot \frac{d}{l})^{\frac{1}{3}} \cdot (\frac{\mu_f}{\mu_w}) \tag{8}$$

When flow is turbulent, Gnielinski formula is used expression of Nusselt number.

$$Nu = \frac{(f/8)(Re - 1000) \cdot Pr}{1 + 12.7\sqrt{\left(\frac{f}{8}\right)} \cdot \left(Pr^{\frac{2}{3}} - 1\right)} \left(1 + \left(\frac{d}{l}\right)^{2/3}\right) \cdot \left(\frac{Pr_f}{Pr_w}\right)^{0.01} \tag{9}$$

$$f = (1.82 lgRe - 1.64)^{-2} \tag{10}$$

The Reynolds number is defined as follows.

$$Re = \frac{\rho \cdot u \cdot l}{\mu} \tag{11}$$

The total resistance of pipe can be calculated by following relations.

$$F_{total} = F_{linear} + F_{part} \tag{12}$$

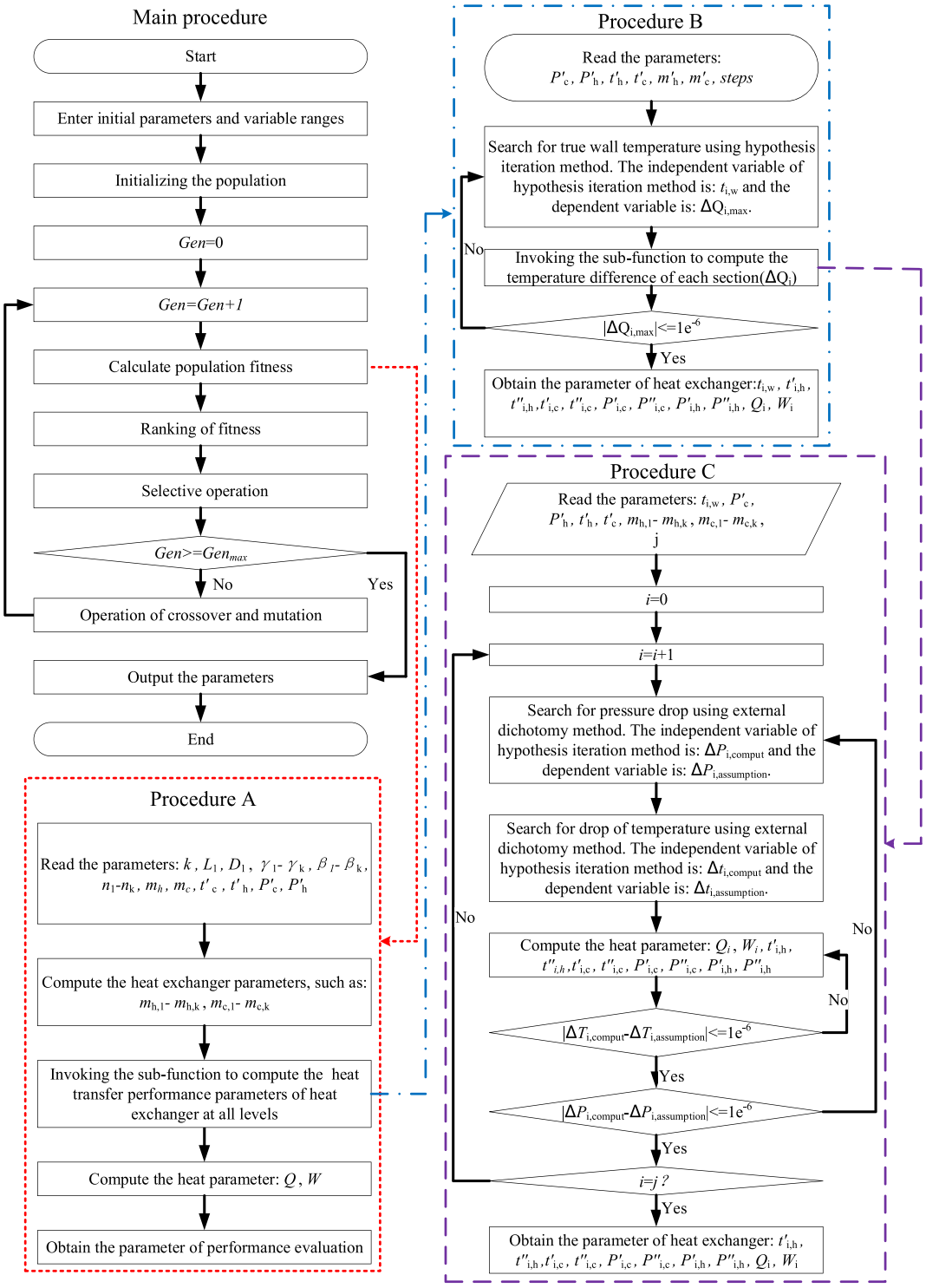

Fig. 4. Thermal design methods of heat transfer structure.

The resistance along path can be calculated by following relations.

$$F_{\text{linear}} = \zeta \frac{l \cdot u^2}{2 \cdot d \cdot g} \tag{13}$$

When flow is turbulent, resistance factor proposed by Petukhov [31] is adopted to calculate resistance coefficient along path.

$$\zeta = (0.79 \cdot \ln(Re - 1.64))^{-2} \tag{14}$$

When the flow is laminar, drag coefficient along path is calculated by following relations.

$$\zeta = \frac{64}{Re} \tag{15}$$

The calculation of local resistance is as follows.

$$F_{\text{part}} = \varepsilon \frac{u^2}{2 \cdot g} \tag{16}$$

The bifurcated model is shown in Fig 5.

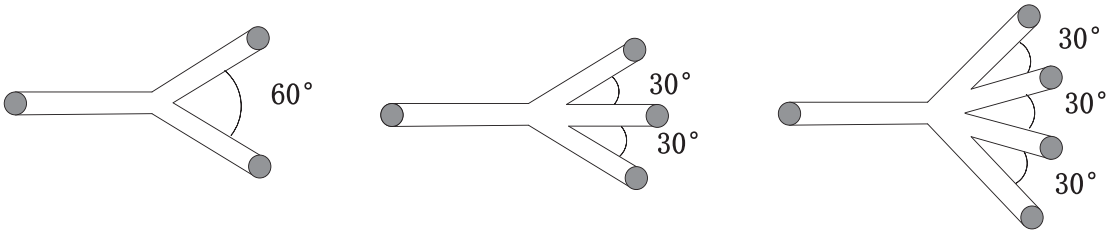

Fig. 5. Bifurcated model.

Table 1
Coefficient of local drag.

Number of branches	Coefficient of local drag
2	1.12
3	2.37
4	3.49

The local resistance coefficient is a function of the structure, number of bifurcations, bifurcation angle, and hydraulic diameter. Typically, an increase in the number of branches results in an increase in the coefficient, but the growth rate may vary. Although this variability may impact the specific value of the coefficient, it will not alter the overall trend. Experimental and numerical simulation methods can provide accurate and reliable values for local resistance coefficients. In engineering calculations, the local resistance coefficients in the Practical Fluids Manual [32] are frequently employed and possess a certain degree of reliability. The model employed in this study comprises uniform and symmetrical branches with uniform traffic distribution. As per the Practical Fluids Manual, the value of the local resistance coefficient corresponding to the number of branches can be obtained under the same flow area for each branch. For applications that require calculation accuracy, it is recommended to use the local resistance coefficient value in the calculation background. The values of the local resistance coefficient are shown in Table 1.

The total power consumption of heat transfer structure is calculated by

$$W = \rho_h \cdot g \cdot \dot{m}_h \cdot F_{h,total} + \rho_c \cdot g \cdot \dot{m}_c \cdot F_{c,total} \tag{17}$$

The Nusselt number, factor of resistance, Stanton number, and pressure drop are commonly used indicators to indirectly reflect the heat transfer performance of a structure, as described by He et al. [33]. However, in order to evaluate accurately the performance of the heat transfer structure, its heat transfer and power consumption are directly measured and analyzed.

$$E = \alpha \frac{(Q) - (Q_{min})}{(Q_{max}) - (Q_{min})} + \beta \frac{\left(\frac{1}{W}\right) - \left(\frac{1}{W}\right)_{min}}{\left(\frac{1}{W}\right)_{max} - \left(\frac{1}{W}\right)_{min}} + \gamma \frac{\left(\frac{Q}{W}\right) - \left(\frac{Q}{W}\right)_{min}}{\left(\frac{Q}{W}\right)_{max} - \left(\frac{Q}{W}\right)_{min}} \tag{18}$$

The performance index of the heat transfer structure is represented by E, which is obtained by normalizing and weighting the efficiency, heat transfer, and power consumption of the structure. The weights assigned to each component are denoted by α, β, and γ, each of which is taken as 1/3 to reflect the equal importance of each target.

3. Results and discussion

The present study firstly analyzes the influence of parameters and flow direction on the heat transfer performance of fractal heat transfer structures. To optimize the length ratio, diameter ratio, and number of branches at all levels of the heat transfer structure simultaneously, a genetic algorithm is employed, representing a significant advancement in related research fields.

3.1. Validation of mathematical model

Research on counter-current fractal heat exchangers is lacking, and to ensure the accuracy of the mathematical model, the heat transfer parameters of a counter-current straight channel [27] were used for verification. Table 3 summarizes the comparison of results between the literature and the mathematical model, indicating that the maximum error did not exceed 6%. The investigation of heat transfer characteristics of two-fluid fractal structures and the optimization methods for improving their performance are currently the main research directions. Therefore, the acceptable level of error is reasonable.

3.2. Comparison of heat transfer performance between co-current and counter-current

In the process of analysis, the fixed parameters including flow direction, length ratio at all levels, diameter ratio at all levels, number of branches at all levels, temperature and pressure of fluids at inlet, and other calculation parameters are given. Values of fixed parameter as shown in Tables 4 and 5. The specific length, diameter, and branch number of numerical references Murray's law and its derivation [34].

As depicted in Fig. 6(a), the temperature profile of supercritical CO_2 in co-current pattern differs from that of the counter-current pattern. Specifically, the temperature of the former is lower in the first half and higher in the latter half compared to the latter. This behavior can be attributed to the large temperature difference between the inlet hot and cold fluids in the co-current pattern, leading to a more efficient cooling effect of supercritical CO_2. However, in the last half part of the co-current pattern, the temperature difference between the hot and cold fluids is smaller, resulting in a lower temperature of supercritical CO_2 than that of the counter-current pattern. As shown in Fig. 6(b) and (c), the wall temperature of the fractal counter-current model fluctuates near the average temperature of the hot and cold fluids along the flow direction. Additionally, the wall temperature decreases continuously with decreasing temperature of the hot fluid. Notably, the wall temperature is higher in the high temperature section, which necessitates higher material requirements for the heat transfer structure. It is also worth mentioning that the wall temperature of the fractal heat transfer structure exhibits sharp changes at bifurcations. Since the absolute temperature of supercritical CO_2 is less than 374 K, the manufacturing process does not pose significant challenges.

In the counter-current pattern, the entrance effect of H_2O in the initial segment of the next level is relatively weak. As a result, the thermal resistance of the H_2O side in this segment is higher than that of the last segment of the level above it. This leads to a higher temperature difference between the H_2O and wall surface compared to the last segment of the level above. Furthermore, the temperature of the wall exhibits a slightly upward trend in this

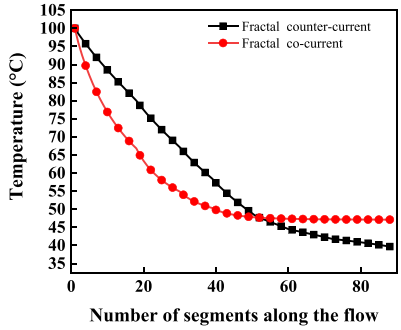

(a) Distribution of supercritical CO_2 temperature along flow direction.

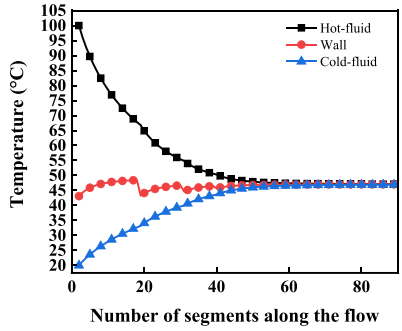

(b) Temperature distribution along flow direction of wall and fluid in co-current pattern.

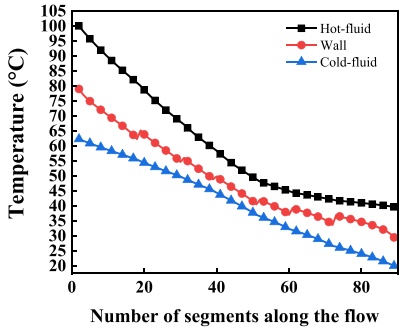

(c) Temperature distribution along flow direction of wall and fluid in counter-current pattern.

Fig. 6. Temperature distribution along flow direction in heat transfer structure.

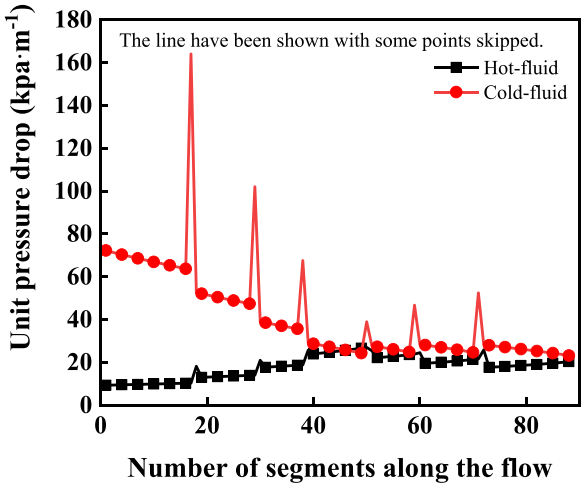

Fig. 7. The distribution of unit pressure drop along flow direction in counter-current pattern.

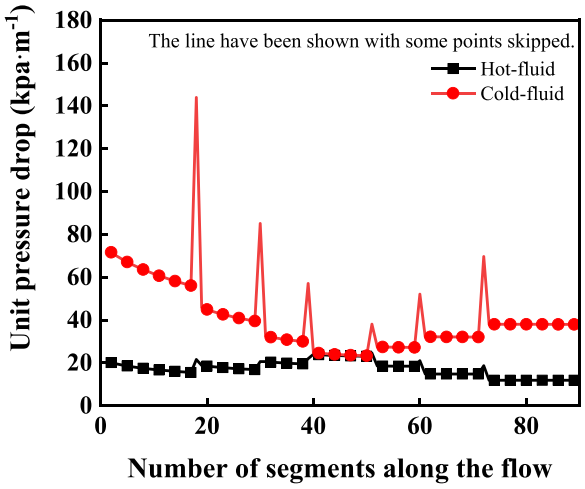

Fig. 8. The distribution of unit pressure drop along flow in co-current pattern.

scenario. On the other hand, in the co-current pattern, the impact of the entrance effect on turbulence is less pronounced than that on laminar flow when the inlet length is the same. Consequently, the thermal resistance of supercritical CO_2 in turbulent flow becomes larger, leading to an increased temperature difference between the supercritical CO_2 and wall. In this case, the wall temperature exhibits a slightly downward trend.

As shown in Figs. 7 and 8, the loss of local resistance caused by bifurcation leads to a substantial increase in pressure drop along the flow path. At the beginning of a branch, the mass flow and velocity of each tube decrease significantly due to the split-flow of the branch. In this context, it is important to note that the pressure drop primarily depends on the velocity of the fluid. Therefore, the pressure drop of the initial segment of the next level branch of supercritical CO_2 is significantly lower than that of the last segment of the level above it

As shown in Fig. 9, the velocity of cold and hot fluids decreases significantly at the same level, primarily as a function of the fluid's density. The density of H_2O is minimally impacted by changes in temperature and pressure, resulting in minimal variation in velocity at the same level. In contrast, the density of supercritical CO_2 is strongly influenced by changes in temperature and pressure. Specifically, as the temperature of supercritical CO_2 decreases and pressure increases, its density increases accordingly. The velocity of supercritical CO_2 at the same level is positively correlated with the direction of density change.

As shown in Figs. 10 and 11, as the inlet mass flow rate increases, the fluid velocity increases continuously. The quantity of heat transferred and the power consumption are positively correlated with the fluid velocity, resulting in an overall increasing trend. It is important to note that the heat transfer efficiency in counter-current mode is consistently superior to that of co-current mode. Furthermore, the power consumption of the counter-current mode is typically slightly greater than that of the co-current mode.

As depicted in Fig. 12(a), in the next branch, the heat transfer area is the primary factor that determines the thermal resistance. The total thermal resistance suddenly decreases as the heat transfer area increases significantly. Conversely, in the next confluence, the heat transfer area is greatly reduced, and the total thermal resistance suddenly increases. In counter-current flow, the thermal resistance of supercritical CO_2 mainly depends on the entrance effect and fluid thermal conductivity. The entrance effect decreases

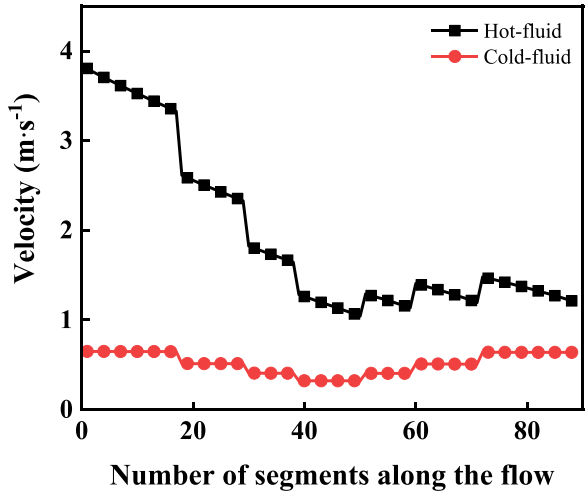

Fig. 9. The distribution of velocity along flow in counter-current pattern.

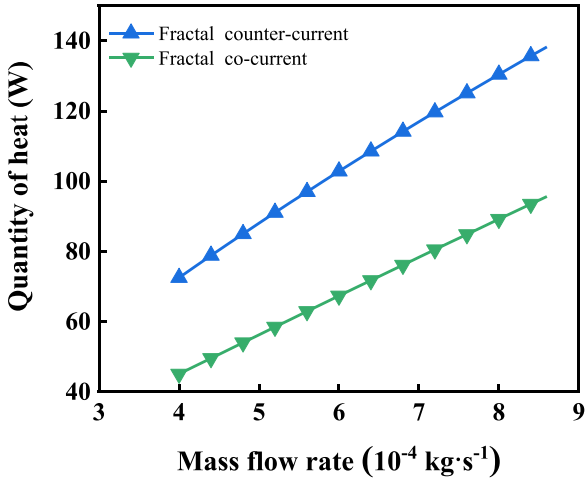

Fig. 10. The heat transfer of fractal structure varies with inlet mass flow rate.

along the path, and the thermal conductivity of supercritical CO_2 increases as the temperature along the path decreases. In the initial stage of each level, the weakening of the entrance effect plays an important role, and the thermal resistance of the supercritical CO_2 side increases along the path. After the middle section of each level, the increase of thermal conductivity of supercritical CO_2 plays a major role, and the thermal resistance of the supercritical CO_2 side decreases along the path. Under the joint influence of the entrance effect and fluid thermal conductivity, the thermal resistance of supercritical CO_2 first increases and then decreases. On the contrary, the flow direction of counter-current H_2O is opposite to that of supercritical CO_2, and the influence of the entrance effect is inversely proportional to that of the supercritical CO_2 side. Therefore, under the joint action of the entrance effect and fluid thermal conductivity, the thermal resistance along the direction of the supercritical CO_2 flow shows a decreasing trend, and the decreasing rate is consecutively increasing. The total thermal resistance in counter-current flow is composed of the thermal resistance of the supercritical CO_2 side and H_2O side. Therefore, the total thermal resistance in the counter-current flow mode shows an increasing trend first and then a decreasing trend. When the flow is co-current, the thermal resistance of supercritical CO_2 first increases and then decreases. Under the joint action of the entrance effect and fluid thermal conductivity, the thermal resistance of H_2O will continuously increase along the path. Under the influence of

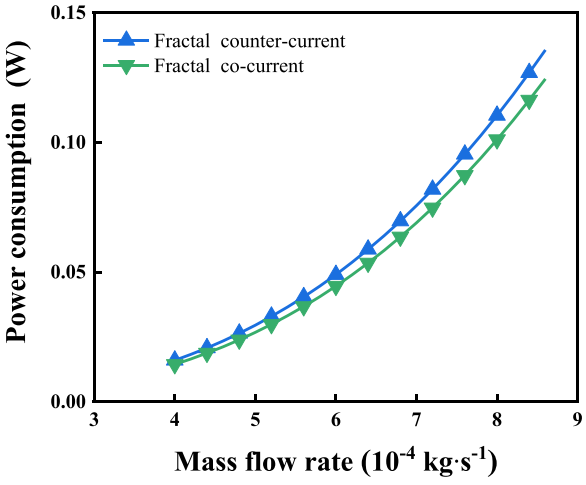

Fig. 11. The power consumption of fractal structure varies with inlet mass flow rate.

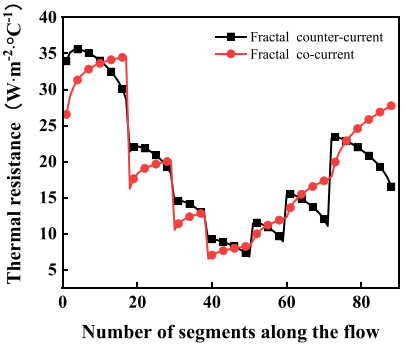

(a) Thermal resistance distribution along the path of fractal heat transfer structure.

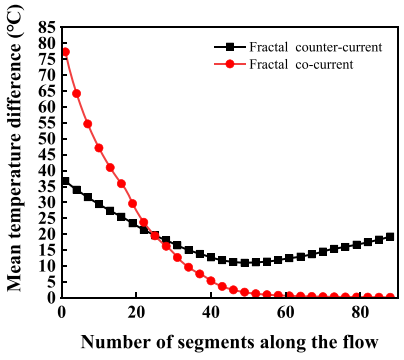

(b) Mean temperature difference distribution along the path of fractal heat transfer structure.

Fig. 12. Variation of heat transfer index along fractal heat transfer structure path.

the thermal resistance of hot and cold fluids, the total thermal resistance will continuously increase.

As shown in Fig. 12(b), the co-current fractal heat transfer structure achieves a larger heat transfer temperature difference in the initial quarter section, but the mean heat transfer temperature difference fluctuates greatly along the path. The mean heat transfer temperature difference in the last half section is too low, whereas the mean heat transfer temperature difference of the counter-current structure shows a stable trend. The calculation found that the quantity of heat in the counter-current mode is 24.4% higher than that in the co-current mode. The mean temperature difference of the counter-current fractal heat transfer structure is 24% higher than that in the co-current fractal heat transfer structure.

Table 2
Parameters of the counter-current straight channel [27].

	Medium	Parameter	Unit	Value
Hot fluid	Supercritical CO_2	Mass flow	$kg{\cdot}s^{-1}$	0.2×10^{-3}
		Temperature of Inlet and outlet	°C	76.2, 34.4
		Pressure drop of Inlet and outlet	bar	82.17, 79.87
Cold fluid	H_2O	Mass flow	$kg{\cdot}s^{-1}$	0.3×10^{-3}
		Temperature of Inlet and outlet	°C	25, 50
		Pressure drop	bar	TBD
		Quantity of heat	W	37.87
		Hydraulic Diameter	m	0.0015
		Length	m	0.96

Thus, the mean temperature difference of the counter-current heat transfer structure is the main factor impacting the quantity of heat.

3.3. Influence of fractal heat transfer structure parameters on heat transfer performance

In the process of analyzing the influence of fractal heat transfer structure parameters on heat transfer performance, the values of fixed parameters are shown in Tables 2 and 3. By controlling variation of each structural parameter within a reasonable range, the influence law of each parameter on the performance of fractal heat transfer structure can be obtained.

As depicted in Fig. 13(a), the impact of the number of branches on the performance of the fractal heat transfer structure can be observed. When the number of branches changes, the total heat transfer is composed of the heat transfer of each branch pipe and the number of branch pipes. The total heat transfer is positively correlated with both factors. However, as the number of branches increases, the branch pipes also increase significantly. Consequently, the heat transfer of each branch pipe decreases due to the decreased flow of each branch. Under the joint influence of the number of branch pipes and heat transfer of each branch pipe, the total quantity of heat increases initially and then decreases.

As illustrated in Fig. 13(b), with an increase in the number of level 2 branches, power consumption initially decreases and then increases. The power consumption of the fractal structure is affected by two main factors: frictional resistance and local resistance. As the number of branches increases, the frictional resistance reduces due to the decrease of mass flow rate, while the value of local resistance coefficient increases. Under the joint action of the local resistance and frictional resistance along the path, there will be an optimal number of branches in each level to minimize power consumption.

From Fig. 13(c), it can be observed that the influence trend of the change in the number of level 3 branches on power consumption and heat transfer performance is similar to that of changes in the number of level 2 branches and level 1 branches. However, under the joint influence of the number of branch pipes and heat transfer of each branch pipe, the total heat transfer decreases initially and then increases. In summary, there is an optimal number of branches in each level that can maximize the index of heat transfer performance and minimize power consumption of the entire heat transfer structure.

Fig. 14(a) illustrates that with an increase in the length ratio of level 1, the quantity of heat and power consumption show an increasing trend due to the increase in frictional resistance along the path and heat transfer area. Under the joint action of heat transfer and power consumption, the index of heat transfer performance exhibits a trend of first increasing and then decreasing. It is worth noting that when the length of the pipe increases continuously, the

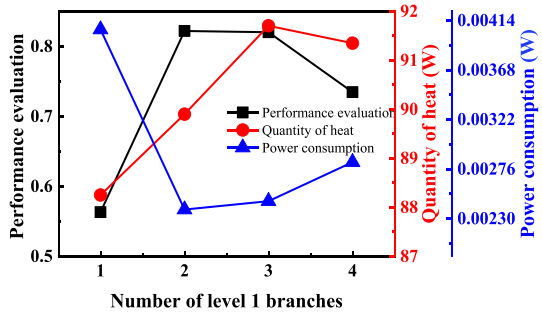

(a) Variation of heat transfer performance with number of level 1 branches

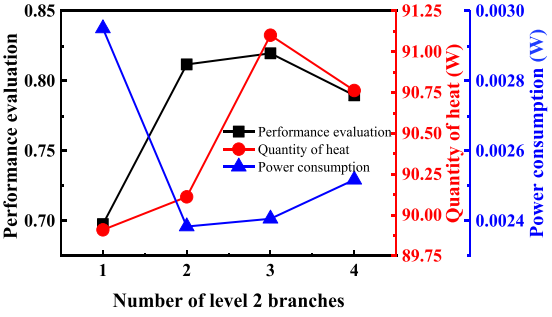

(b) Variation of heat transfer performance with number of level 2 branches

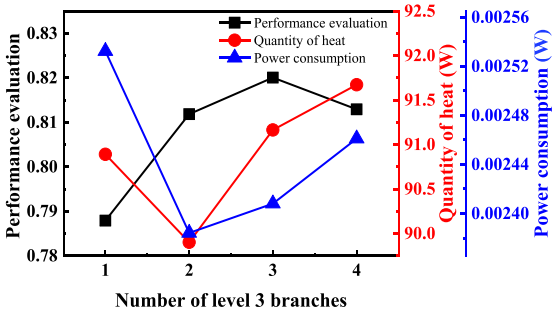

(c) Variation of heat transfer performance with number of level 3 branches

Fig. 13. Variation of performance of fractal heat transfer structure with branch number.

entrance effect of the fluid decreases continuously, resulting in a decrease in the rate of increase of heat transfer.

As shown in Fig. 14(b) and 14(c), the influence trend of variational level 2 length ratio and level 3 length ratio on power consumption and index of heat transfer performance is similar to the influence trend of variational level 1 length ratio.

It can be observed from Fig. 15(a) that the quantity of heat first increases and then decreases as the level 1 diameter ratio increases. When the diameter ratio changes, the quantity of heat depends on both the heat transfer area and the mass flow rate, with the magnitude of heat transfer being positively correlated with both of them. As the level 1 diameter ratio increases, the heat transfer area increases, and the mass flow rate decreases. When the diameter ratio is small, heat transfer is greatly affected by the heat transfer area. However, as the diameter ratio increases, the influence of flow velocity on heat transfer gradually becomes dominant, resulting in the maximum value of heat transfer. The power consumption decreases with the level 1 diameter ratio increase, but the increase in trend is gradual. When the diameter ratio changes, the flow velocity becomes the dominant factor in determining the power consumption of the fractal structure. The flow

Table 3
Comparison of results between literature and mathematical model.

	Quantity of heat (W)	Pressure drop (kPa)	Temperature of outlet (°C)
Literature results	37.87	3.7	34.4
Mathematical modeling results	35.77	3.63	36.62
Residual error	5.5%	1.8%	6.0%

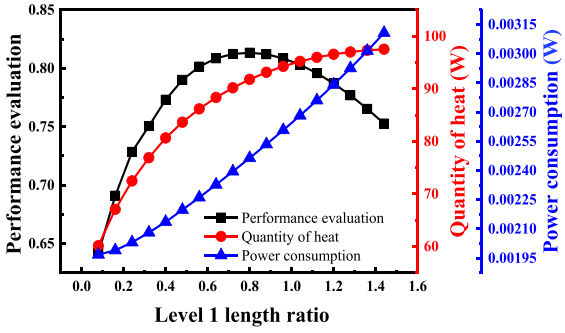

(a) Variation of heat transfer performance with level 1 length ratio

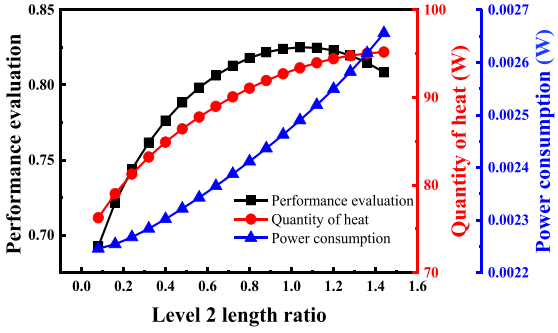

(b) Variation of heat transfer performance with level 2 length ratio

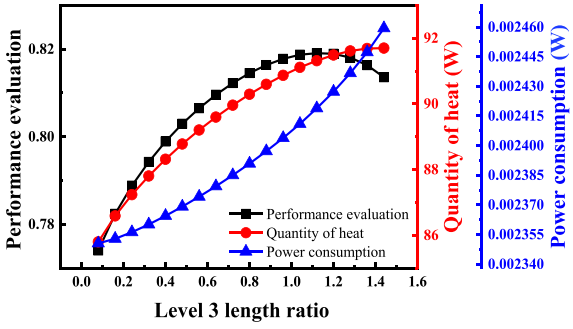

(c) Variation of heat transfer performance with level 3 length ratio

Fig. 14. Variation of heat transfer performance of fractal heat transfer structure with length ratio.

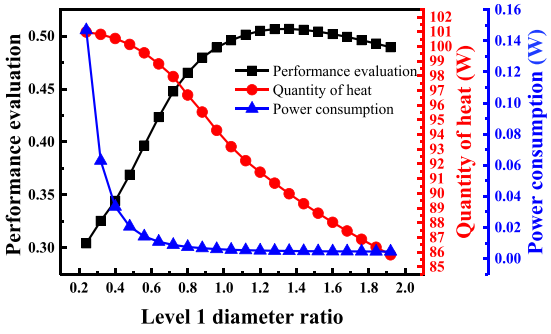

(a) Variation of heat transfer performance with level 1 diameter ratio

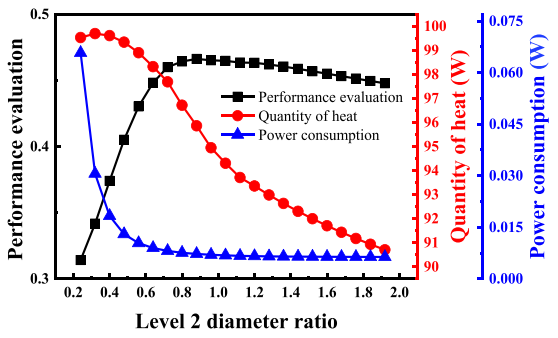

(b) Variation of heat transfer performance with level 2 diameter ratio

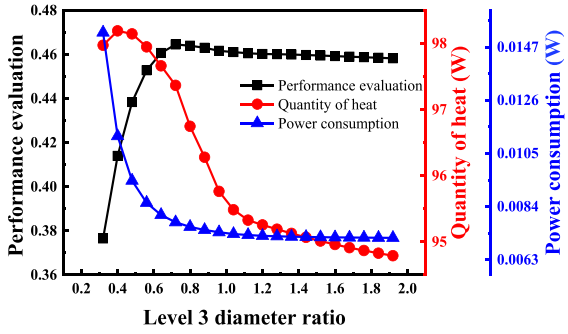

(c) Variation of heat transfer performance with level 3 diameter ratio

Fig. 15. Variation of heat transfer performance of fractal heat transfer structure with diameter ratio.

velocity decreases as the pipe diameter ratio increases, and the decrease rate of flow velocity also decreases. As shown in Fig. 15(b) and 15(c), the influence of the variational level 2 diameter ratio and level 3 diameter ratio on the quantity of heat, power consumption, and performance index is similar to the influence trend of the variational level 1 length ratio.

3.4. Optimization of fractal heat transfer structure parameters

The heat transfer performance of the fractal structure has been analyzed, and it has been concluded that varying the length, diameter, and number of branches at each level has a distinct influence on the heat transfer, power consumption, and heat transfer performance index of the structure, under the condition that other parameters are held constant. It is widely recognized that a heat transfer structure should aim to achieve low power consumption and high heat transfer efficiency. Consequently, in this study, the pipe length, pipe diameter ratio, and branch number at each level were taken as optimization variables, and multi-objective optimization was carried out on the heat transfer structure to achieve enhanced heat transfer performance. The design parameters and

Table 4
Fixed fluid parameters of fractal heat transfer structure [27].

	Medium	Parameter	Unit	Value
Hot fluid	Supercritical CO_2	Mass flow	$kg{\cdot}s^{-1}$	0.5×10^{-3}
		Temperature of inlet	°C	100
		Pressure of inlet	MPa	9.1
Cold fluid	H_2O	Mass flow	$kg{\cdot}s^{-1}$	0.5×10^{-3}
		Temperature of inlet	°C	20
		Pressure of inlet	MPa	0.1

Table 5
Fixed parameters of fractal heat transfer structure [27,34].

Parameter	Unit	Value
Length of level 1	m	0.1
Diameter of level 1	m	0.001
Number of branches at all levels	/	2
Levels	/	4
Length ratio of all levels	/	0.707
Diameter ratio of all levels	/	0.793

Table 5
Parameters of fractal heat transfer structure.

Parameter	Unit	Value
Length of level 1	m	0.1
Diameter of level 1	m	0.001
Levels	/	4
Number of branches at all levels	/	2-4
Length ratio of all levels	/	0-1
Diameter ratio of all levels	/	0-1

Table 6
Optimized parameters of structure of fractal heat structure.

Parameter	Unit	Value
Length of level 1	m	0.1
Diameter of level 1	m	0.001
Levels	/	4
Number of branches at all levels	/	2,3,3
Length ratio of all levels	/	0.93,0.67,0.48
Diameter ratio of all levels	/	0.98,0.97,0.63

Table 7
Comparison of heat transfer performance structure between before and after optimization.

	Quantity of heat (W)	Power consumption (W)	Index of heat transfer performance
Before optimization	89.90	0.0023	0.79
After optimization	92.10	0.0020	0.92
Optimization rate	2.4%	15%	17%

optimization parameters of the heat transfer structure are presented in Table 4, and the parameters after optimization are shown in Table 5.

Table 7 summarizes the comparison of every heat transfer performance between before and after optimization. It can be found evidently that power consumption of the optimized heat transfer structure has reduced by 15%. The heat transfer has increased by 2.4%. The index of heat transfer performance has improved by 17%. The comprehensive performance of optimized heat transfer structure is significantly better than that before optimization (Tables 6,5).

4. Conclusions

Based on the principles of biomimicry, this study proposes an optimization method for a two-fluid fractal heat transfer structure. The fluids are supercritical CO_2 and H_2O, The main conclusions of this investigation are as follows.

(1) Under the same design parameters, the power consumption and heat transfer rate of the counter-current fractal heat transfer structure are always better than those of the co-current fractal heat transfer structure.
(2) Heat transfer rate increases with the number of branches when other structural parameters are constant. Power consumption decreases at first and then increases as the number of branches increases. The heat transfer performance index initially increases and then decreases, reaching an optimal value with an increase in the number of branches. Power consumption and heat transfer rate increase continuously with an increase in pipe length. Heat transfer performance index increases initially and then decreases, reaching an optimal value with an increase in pipe length. Power consumption and heat transfer rate decrease continuously with an increase in pipe diameter. Heat transfer performance index increases initially and then decreases, reaching an optimal value with an increase in pipe diameter.
(3) The results show that power consumption has decreased by 15%, heat transfer has increased by 2.4%, and the heat transfer performance index has improved by 17%. The comprehensive performance of the fractal heat transfer structure is significantly better than that before optimization.

Declaration of Competing Interest

The authors declare that they have no known competing financial interests or personal relationships that could have appeared to influence the work reported in this paper.

CRediT authorship contribution statement

Lisheng Pan: Supervision, Writing – review & editing, Conceptualization. **Zikang Yao:** Conceptualization, Methodology, Data curation, Writing – original draft, Writing – review & editing. **Wei Yao:** Supervision. **Xiaolin Wei:** Supervision, Funding acquisition.

Data availability

The authors are unable or have chosen not to specify which data has been used.

Acknowledgements

This study was supported by National Natural Science Foundation of China (51776215).

References

[1] W. Du, J. Zhao, L. Zhang, Review and prospect of the development of heat exchanger structure, J. Shandong Univ. 51 (05) (2021) 76–83.
[2] T. Ishizuka, Y. Kato, Y. Muto, K. Nikitin, H. Hashimoto, Thermal-hydraulic characteristic of a printed circuit heat exchanger in a supercritical CO_2 loop, in: Proceedings of the 11th International Topical Meeting on Nuclear Reactor Thermal-Hydraulics, 2007.
[3] E.K. Dong, M.H. Kim, J.E. Cha, Numerical investigation on thermal–hydraulic performance of new printed circuit heat exchanger model, Nucl. Eng. Des. 238 (12) (2008) 3269–3276.
[4] I.H. Kim, H.C. No, Physical model development and optimal design of PCHE for intermediate heat exchangers in HTGRs, Nucl. Eng. Des. 243 (2012) 243–250.
[5] T.L. Ngo, Y. Kato, K. Nikitin, T. Ishizuka, Heat transfer and pressure drop correlations of microchannel heat exchangers with S-shaped and zigzag fins for carbon dioxide cycles, Exp. Therm Fluid Sci. 32 (2) (2008) 560–570.

[6] T.L. Ngo, Y. Kato, K. Nikitin, N. Tsuzuki, New printed circuit heat exchanger with S-shaped fins for hot H_2O supplier, Exp. Therm. Fluid Sci. (2006).
[7] N. Tsuzuki, Y. Kato, K. Nikitin, T. Ishizuka, Advanced microchannel heat exchanger with S-shaped fins, J. Nucl. Sci. Technol. 46 (5) (2009) 403–412.
[8] M. Saeed, M.H. Kim, Thermal-hydraulic analysis of sinusoidal fin-based printed circuit heat exchangers for supercritical CO_2 Brayton cycle, Energy Convers. Manage. 193 (2019) 124–139.
[9] X. Xu, T. Ma, L. Li, M. Zeng, Y. Chen, Y. Huang, Optimization of fin arrangement and channel configuration in an airfoil fin PCHE for supercritical CO_2 cycle, Appl. Therm. Eng. 70 (2014) 867–875.
[10] F. Chen, L. Zhang, X. Huai, J. Li, H. Zhang, Z. Liu, Comprehensive performance comparison of airfoil fin PCHES with NACA OOXX series airfoil, Nucl. Eng. Des. 315 (2017) 42–50.
[11] T. Zhang, J.T. Wen, A. Julius, Stability analysis and maldistribution control of two-phase flow in parallel evaporating channels, Int. J. Heat Mass Transf. 54 (25) (2011) 5298–5305.
[12] N.H. Kim, S.P. Han, Distribution of air-H_2O annular flow in a header of a parallel flow heat exchanger, Int. J. Heat Mass Transf. 51 (56) (2008) 977–992.
[13] D. Pence, Reduced pumping power and wall temperature in microchannel heat sinks with fractal-like branching channel networks, Microscale Thermophys. Eng. 6 (2003) 319–330.
[14] M. Xin, B. Hong, Heat transfer performanceand optimization design of double layer Y-shaped bifurcation bionic microchannel, Sci. Technol. Eng. 18 (2018) 112–117.
[15] X.Q. Wang, X. Peng, A.S. Mujumdar, C. Yap, Flow and thermal characteristics of offset branching network, Int. J. Therm. Sci. 49 (2010) 272–280.
[16] D. Pence, Reduced pumping power and wall temperature in microchannel heat sinks with fractal tree like branching channel networks, Microscale Thermophys. Eng. 6 (2003) 319–330.
[17] P. Yi, Research on Bionic Soaking Plate Based on Plant Leaf Structure, South China University of Technology, 2015.
[18] G.Q. Xu, M. Wang, Z Tao Numerical analysis of flow and heat transfer characteristics of Y-shaped micro runner, J. Beijing Univ. Aeronaut. Astronaut. 35 (2009) 313–317.
[19] C. Hong, H. Ge, Conjugate heat transfer in tree–shaped microchannel network heat sink for integrated microelectronic cooling application, Int. J. Heat Mass Transf. 50 (2007) 4986–4998.
[20] J. Qin, Research on Structure Optimization and Flow and Heat Dissipation Characteristics of Bionic Micro channel Radiator, University of Electronic Science and Technology of China, 2012.
[21] D. Kang, W. Shen, Y.P. Zhao, The optimization of material utilization efficiency in fractal flow channels of the microreactor, Sci. Sin. Technol. 49 (2019) 1159–1167.
[22] Z. Tang, L. Sun, C. Qi, Y. Wang, Flow and heat transfer characteristics of a fractal microchannel heat sink with three-dimensional fractal tail, Chem. Eng. 17 (2022) e2803.
[23] X. Ji, X. Yang, Y. Zhang, Experimental study of ultralow flow resistance fractal microchannel heat sinks for electronics cooling, Int. J. Heat Mass Transf. 179 (2022) 107723.1–107723.13.
[24] Y. Yan, H. Yan, S. Feng, Thermal-hydraulic performances and synergy effect between heat and flow distribution in a truncated doubled-layered heat sink with Y-shaped fractal network, Int. J. Heat Mass Transf. 142 (2019) 118337.1–118337.13.
[25] S. Yu, M.J. Lu, W. Wei, Analysis and review on the development of S-CO_2 breton cycle power generation technology with waste heat from ship flue gas, Shipbuild. China 62 (2021) 254–265.
[26] V. Dostal, P. Hejzlar, M.J. Driscoll, High-performance supercritical CO_2 cycle for next-generation nuclear reactors, Nucl. Technol. 154 (2006) 265–282.
[27] J. Lian, D. Xu, H. Chang, Z. Xu, T. Ma, Thermal and mechanical performance of a hybrid printed circuit heat exchanger used for supercritical CO_2 Brayton cycle, Energy Convers. Manage. 245 (2021) 114573.
[28] A. Jolly, T. OD, C. Bates, COHEX: a computer model for solving the thermal energy exchange in an ultra high temperature heat exchanger, Part A: computational theory, Appl. Therm. Eng. 18 (1998) 389–398.
[29] M. Saeed, A.S. Berrouk, M. Salman, A. Ali, Effect of printed circuit heat exchanger's different designs on the performance of supercritical CO_2 brayton cycle, Appl. Therm. Eng. 179 (2020) 1–43.
[30] Y. Lei, S. Zhang. MATLAB Genetic Algorithm Toolbox and Application. 2014.
[31] B.S. Petukhov. Advances in heat transfer. Laminar Flow Forced Convection in Ducts, 1978.
[32] , S.Z. Hua, X.N. Yang. Practical handbook of fluid resistance, National Defense Industry Press, 1985.
[33] Y.L. He, W.Q. Tao, Research progress on comprehensive evaluation indicators of heat exchange equipment. China Society of Engineering Thermophysics, 2011.
[34] Y. Yan, H. Yan, S. Yin, Single/multi-objective optimizations on hydraulic and thermal management in micro-channel heat sink with bionic Y-shaped fractal network by genetic algorithm coupled with numerical simulation, Int. J. Heat Mass Transf. 129 (2019) 468–479.